Fusing Microwave and Optical Satellite Observations to Simultaneously Retrieve Surface Soil Moisture, Vegetation Water Content, and Surface Soil Roughness

Yohei Sawada, Toshio Koike, Kentaro Aida, Kinya Toride, and Jeffrey P. Walker

***Abstract*— Uncertainty in surface soil roughness strongly degrades the performance of surface soil moisture (SSM) and vegetation water content (VWC) retrieval from passive microwave observations. This paper proposes an algorithm to objectively determine the surface soil roughness parameter of the radiative transfer model by fusing microwave and optical satellite observations. It is then demonstrated in a semiarid in situ observation site. The roughness correction of this new algorithm positively impacted the performance of SSM (root-mean-square error reduced from 0.088 to 0.070) and VWC retrieval from the Advanced Microwave Scanning Radiometer 2 and Moderate Resolution Imaging Spectroradiometer. Since this surface soil roughness correction may be transferrable to other microwave satellite retrieval algorithms such as those for the Soil Moisture and Ocean Salinity and Soil Moisture Active Passive satellites, this new algorithm can contribute to many microwave earth surface observation satellite missions.**

***Index Terms*— Microwave radiometry, satellite applications, soil, vegetation, water resources.**

I. Introduction

PASSIVE microwave satellite observations have greatly contributed to global surface soil moisture (SSM) observations (see [1]–[3]). Global SSM products from satellite-based microwave observations have widely been used to quantify drought impacts (see [4]), analyze land–atmosphere interactions (see [5]), and improve the soil moisture simulation of a land surface model by data assimilation (see [6], [7]). In addition, microwave data are useful for monitoring terrestrial vegetation dynamics since the microwave vegetation optical depth (VOD) is highly sensitive to vegetation water content (VWC) [8]. This sensitivity of a microwave signal to terrestrial vegetation dynamics has been utilized to analyze the global carbon cycle [9], monitor the change of the rainforest (see [10]), and improve the performance of an ecohydrological model by data assimilation [11], [12].

Despite significant effort to develop the SSM and VWC retrieval algorithms from passive microwave observations [13], there is a need for further improvement in the current algorithms [14]. One of the most critical issues is the uncertainty of surface soil roughness, which greatly affects the microwave radiative transfer on land (see [15]). Consequently, the lack of information about surface soil roughness, which is difficult to directly observe at satellite footprint scales, degrades the SSM and VWC retrieval accuracy. For example, Patton and Hornbuckle [16] indicated that the VOD product from the Soil Moisture and Ocean Salinity (SMOS) mission might strongly be affected by the change of surface soil roughness due to land management activities. Moreover, Njoku and Chan [17] proposed to retrieve a single parameter from the Advanced Microwave Scanning Radiometer for Earth Observation System (AMSR-E) brightness temperature observations to reflect the combined effect of vegetation and surface soil roughness. However, it is difficult to decompose this parameter into the separate VWC and surface soil roughness contributions [17].

Recently, Sawada *et al.* [18] undertook a field experiment that measured SSM, VWC, leaf area index (LAI), and microwave brightness temperatures from a ground-based microwave radiometer, and showed that VWC and surface soil roughness can independently be retrieved by fusing a microwave signal and observed LAI. Wang *et al.* [19] utilized a similar approach to estimate a soil roughness parameter of their radiative transfer model (RTM) at global scale by fusing AMSR-E brightness temperature, the SMOS derived soil moisture product, European Centre for Medium-range Weather Forecasting soil temperature, and Moderate Resolution

Manuscript received April 11, 2016; revised September 18, 2016, December 12, 2016, April 28, 2017, and June 19, 2017; accepted June 21, 2017. Date of publication July 26, 2017; date of current version October 25, 2017. This work was supported in part by the Japan Aerospace Exploration Agency and in part by the Japan Society for the Promotion of Science (JSPS) under KAKENHI Grant JP17K18352. The work of Y. Sawada was supported by the JSPS under Grant 255893. *(Corresponding author: Yohei Sawada.)*

Y. Sawada was with the Department of Civil Engineering, School of Engineering, The University of Tokyo, Tokyo 113-8654, Japan, and also with the Data Assimilation Research Team, RIKEN Advanced Institute for Computational Science, Kobe 650-0047, Japan. He is now with the Forecast Department, Meteorological Research Institute, Japan Meteorological Agency, Tsukuba 305-0052, Japan (e-mail: ysawada@mri-jma.go.jp).

T. Koike is with the Department of Civil Engineering, School of Engineering, The University of Tokyo, Tokyo 113-8654, Japan, and also with the International Centre for Water Hazard and Risk Management, Tsukuba 300-2621, Japan (e-mail: koike@icharm.org).

K. Aida is with the Center for Research in Isotopes and Environmental Dynamics, University of Tsukuba, Tsukuba 305-8571, Japan (e-mail: aida@ied.tsukuba.ac.jp).

K. Toride was with the Department of Civil Engineering, School of Engineering, The University of Tokyo, Tokyo 113-8654, Japan. He is now with the Department of Civil and Environmental Engineering, University of California, Davis, CA 95616 USA (e-mail: kinya.toride@gmail.com).

J. P. Walker is with the Department of Civil Engineering, Monash University, Clayton, VIC 3800, Australia (e-mail: jeff.walker@monash.edu).

Color versions of one or more of the figures in this paper are available online at http://ieeexplore.ieee.org.

Digital Object Identifier 10.1109/TGRS.2017.2722468

Imaging Spectroradiometer (MODIS) normalized difference vegetation index (NDVI). However, Wang *et al.* [19] used the estimated SSM to retrieve the surface soil roughness parameters and did not check if the estimated surface soil roughness parameter can improve the accuracy of the SSM and VWC retrieval. No study has evaluated how these surface soil roughness estimations, from fusing microwave and optical observations, impact the skill of simultaneously retrieved SSM and VWC at the satellite footprint scales.

The aim of this paper is, therefore, to propose a new algorithm to simultaneously retrieve SSM and VWC by fusing the AMSR2 brightness temperature and MODIS-derived LAI. Although the original idea has been proposed in [18], it has not been verified in the real-world satellite observation. Some modifications for applying it to satellite data are described and tested in this paper. The existing concepts used in the Japan Aerospace eXploration Agency (JAXA) standard algorithm are included for the application of satellite observations. This new algorithm addresses the uncertainty of surface soil roughness by introducing optically observed LAI into the microwave retrieved parameter, which reflects the combined effect of vegetation and surface soil roughness. The performance of the algorithm is evaluated using *in situ* soil moisture observation network data and *in situ* observed VWC in a semiarid region.

II. Data

Five satellite and two *in situ* data sets from January 2013 to December 2014 were used. The microwave brightness temperatures used in this paper were measured using the AMSR2 sensor onboard the Global Change Observation Mission-Water satellite (JAXA AMSR2 L3 product). In addition to the brightness temperatures, AMSR2 SSM products and a VOD product were used to compare the retrieved SSM and VOD in this paper with those in the existing algorithms. The SSM product produced by the JAXA standard algorithm [20], [21] (JAXA AMSR2 L3 product; https://gcom-w1.jaxa.jp/auth.html) and the SSM and VOD products produced by the Land Parameter Retrieval Model (LPRM L3 product; https://earthdata.nasa.gov/) [1] were used. Only data of descending (nighttime) pass were used because the vertical temperature gradients are weaker and VOD retrievals can be stable [22], [23].

In this paper, microwave and optical satellite observations are fused to reduce the effect of the uncertainty of surface soil roughness on the microwave radiative transfer. The optical satellite product used in this paper was the MODIS MCD15A3 four-daily LAI product [24] which can be downloaded from https://earthdata.nasa.gov/. All satellite data were resampled to the JAXA AMSR2 L3 product's resolution ($0.1^\circ \times 0.1^\circ$) by the nearest neighbor algorithm. No temporal interpolation has been implemented.

To evaluate the performance of the algorithm developed in this paper, the ground-observed soil moisture data set from a grassland area of the Yanco region, Australia, was used. This data set forms part of the Murrumbidgee Soil Moisture Monitoring Network (http://www.oznet.org.au/) [25]. Our target area is a 9 km $\times$ 9 km area whose central coordinate is approximately (34.9S, 146.3E). This area corresponds to one pixel of the JAXA L3 product. Fig. 1(a) indicates the distribution of soil moisture ground observation sites within the satellite data pixel. Stevens Hydra 5-cm long probes were vertically installed at all sites. These observed soil moistures represent the soil moisture within a depth of 0–5 cm. However, there may be some biases in the observation depths since the measurements are affected by not only soil between the four probes but also soil surrounding the four probes although this effect may be minimal. All the data obtained from these sites were averaged to get the representative *in situ* observed SSM at the satellite footprint scale [26]. The values whose observation time was closest to the time of satellite descending overpasses were used. The *in situ* observed SSM ranged from approximately 0.05 to 0.3 [m^3/m^3].

In addition to soil moisture, *in situ* observations of VWC were undertaken. It should be mentioned that obtaining *in situ* VWC in the satellite footprint scale is extremely difficult due to the spatial heterogeneity of VWC. We have three types of VWC data, Types I, II, and III. The Type I data include a field survey undertaken on July 7, 2014 with eight plots taken around the flux tower [square T1 in Fig. 1(a) and (b)]. The two plots were taken in close proximity of the flux tower. The three sets of two plots were taken in an approximate 100-m northward, eastward, and southward to the flux tower. The Type I data also include a field survey undertaken on October 23 and 24, 2014 with 12 plots taken across the satellite pixel [see Fig. 1(b)]. Because these two surveys had many plots separated from each other, it is assumed that these Type I *in situ* observations can represent the satellite footprint-scale VWC. Moreover, the Type II data consist of the vegetation samplings of three plots around the tower and the Type III data consist of the vegetation samplings of three plots located 2 km from the tower. Field surveys for Type II and Type III were undertaken on February 28, 2014, April 2, 2014, May 6, 2014, and August 12, 2014. Because of the small number of plots and the unsatisfactory spatial coverage, it is difficult to assume the observations of Type II and Type III can represent the satellite footprint-scale VWC. However, the Type II and Type III observations were used to evaluate the skill of this new algorithm to reproduce the temporal dynamics of VWC. These intensive observations include the whole seasonal cycle of vegetation dynamics. The size of all sampling plots was 50 cm $\times$ 50 cm. The VWC was calculated as the difference between the mass of the wet and dry biomass. The *in situ* observed VWC ranged from approximately 0 [kg/m^2] to 1 [kg/m^2]. This study area is dominated by the savanna or grassland ecosystem with some croplands.

III. Method

A. Radiative Transfer Model

The RTM used in this paper has been used in [11], [12], and [18]. As a surface soil emission model, the advanced integral equation model incorporating the shadowing effect developed by Kuria *et al.* [27] was used. This model can be applied to a wide range of surface soil roughness conditions characterized by a root-mean-square (rms) height (σ: cm) and

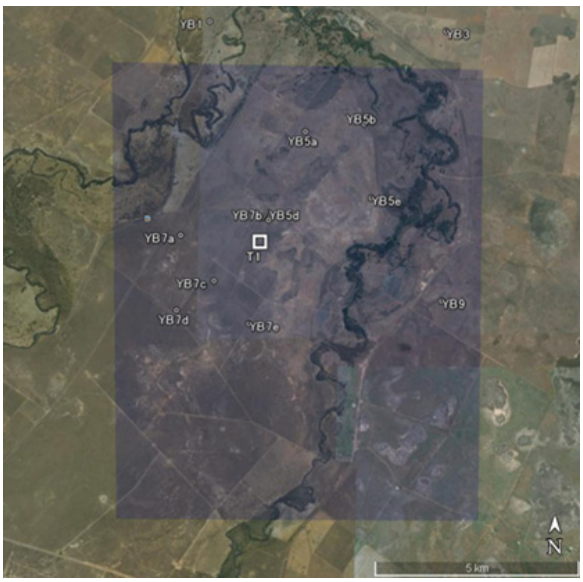

(a)

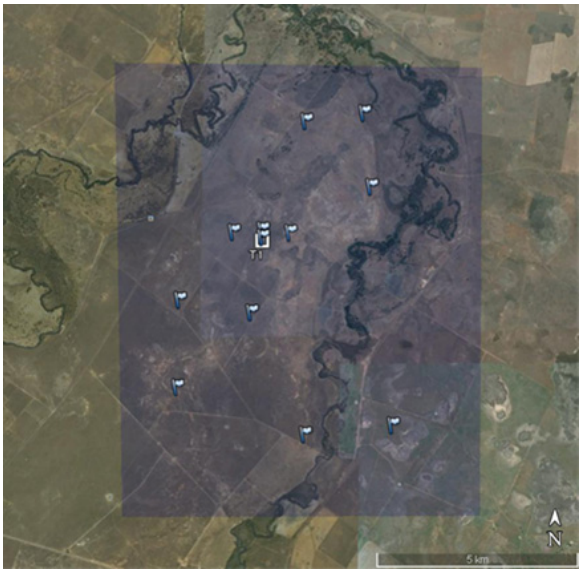

(b)

Fig. 1. Maps of the observation site. (a) Circles (YB1, YB3, ….) are the soil moisture observation sites. The square (T1) is the location of the flux tower. (b) Flags are the VWC observation plots for the survey on October 23 and 24, 2014. The blue transparent rectangle is JAXA's AMSR2 L3 product pixel.

correlation length (l: cm). The explanation of this RTM can be found in [27] and references therein and the important equations are briefly described in this paper. Surface reflectivity can be obtained from

$$R_p = r_p \exp[-(2k\sigma\cos\theta)^2]S(\theta,\theta) + \frac{1}{4\pi\cos\theta}\int_0^{2\pi}\int_0^{\pi/2}[h_{pp}(\theta,\theta_j,\varphi_j)S(\theta,\theta_j) + h_{pq}(\theta,\theta_j,\varphi_j)S(\theta,\theta_j)]\sin\theta_j d\theta_j d\varphi_j \quad (1)$$

where R_p is the surface reflectivity, p and q refer to the polarization state (vertical or horizontal), k is the wavenumber, θ is the incident angle, h is the single scattering terms, θ_j is the scattering direction, φ is the azimuth angle, S is the shadowing function (see [27]), which is dependent on the surface soil roughness parameters [27], and r is the Fresnel reflectivity, which is calculated by

$$r_h = \left|\frac{\cos\theta - \sqrt{\varepsilon_r - \sin^2\theta}}{\cos\theta + \sqrt{\varepsilon_r - \sin^2\theta}}\right|^2 \quad (2)$$

$$r_v = \left|\frac{\varepsilon_r\cos\theta - \sqrt{\varepsilon_r - \sin^2\theta}}{\varepsilon_r\cos\theta + \sqrt{\varepsilon_r - \sin^2\theta}}\right|^2 \quad (3)$$

where ε_r is the dielectric constant of the soil–water mixture (includes both real and imaginary parts) given by

$$\varepsilon_r = [1 + (1-\theta_s)(\varepsilon_s^{\mathrm{A}} - 1) + w^{\beta_R}\varepsilon_{\mathrm{fw}}^{\mathrm{A}} - w]^{1/\mathrm{A}} \quad (4)$$

$$\beta_R = 1.09 - -0.0011\%\ \text{sand} + 0.0018\%\ \text{clay} \quad (5)$$

such that ε_s is the dry soil dielectric constant, θ_s is the saturated soil moisture content, $\varepsilon_{\mathrm{fw}}$ is the dielectric constant of free water, w is the SSM, A = 0.65, and % sand and % clay are the percentages of sand and clay contents in the soil, respectively. The semiempirical equations (4) and (5) are from [28] and [29], respectively. The parameters of these equations (e.g., %sand and %clay) are derived from the default value of the JAXA standard algorithm.

To calculate the total emission from the land surface, the tau–omega model [30] was used to account for the effect of vegetation

$$T_{bp} = (1-R_p)T_s\exp(-\mathrm{VOD}) + (1-\omega_{\mathrm{cp}})T_c(1-\exp(-\mathrm{VOD})) + R_p(1-\omega_{\mathrm{cp}})T_c(1-\exp(-\mathrm{VOD}))\exp(-\mathrm{VOD}) \quad (6)$$

where T_{bp} is the brightness temperature at the radiometer level, T_s is the physical land surface temperature, T_c is the canopy temperature, ω_{cp} is the single scattering albedo of the canopy, and VOD is the vegetation optical depth. The VOD has been found to be linearly related to VWC (VOD = $b \times$ VWC), which was thoroughly verified, although the linear relationship assumption should slightly be modified in the application to a brightness temperature with a higher frequency (e.g., Ka bands) [8], [31]. Please note that in (6) exp(−VOD) is the transmissivity of vegetation at the AMSR2 incidence angle of 55°. The values and uncertainties of important vegetation parameters are discussed in the end of Section III-D.

B. Surface Soil Moisture and Vegetation Optical Depth Retrieval Algorithms

To retrieve SSM and VOD using this RTM, an index of soil wetness (ISW; see [20], [32]) and a polarization index (PI) were used

$$\mathrm{ISW} = \frac{2\left(T_{\mathrm{Bg}}^H - T_{\mathrm{Bf}}^H\right)}{T_{\mathrm{Bg}}^H + T_{\mathrm{Bf}}^H} \quad (7)$$

$$\mathrm{PI} = \frac{2\left(T_{\mathrm{Bf}}^V - T_{\mathrm{Bf}}^H\right)}{T_{\mathrm{Bf}}^V + T_{\mathrm{Bf}}^H} \quad (8)$$

where T_{Bq}^p is the brightness temperature at the radiometer level, superscript p indicates polarizations [vertical (V)

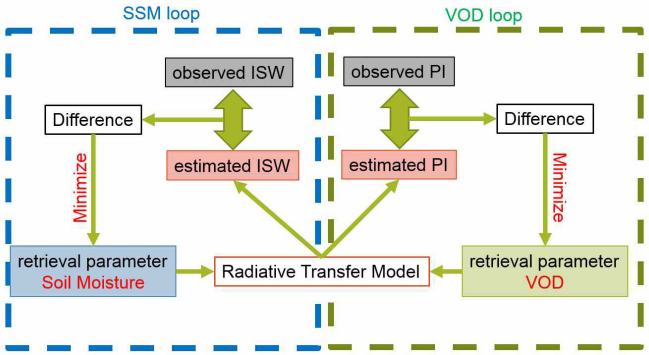

Fig. 2. Schematic of the PI- and ISW-based SSM and VOD retrieval algorithms. See Section III-B for details.

or horizontal (H)], and subscript q indicates frequencies. (g indicates a higher frequency while f indicates a lower frequency.) Since the change in emissivity due to a change in soil moisture strongly depends on the frequency of the microwave observation, ISW is a useful index to estimate SSM. As soil gets wetter, the brightness temperature with a lower frequency decreases more considerably than that with a higher frequency so that ISW increases. In this paper, 36.5 GHz is used as the higher frequency (g) and 6.925 GHz is used as the lower frequency (f). In the case of dry bare soil, the sensing depths of 6.925- and 36.5-GHz observations are on the order of 1 and 0.1 cm, respectively, although there may be some errors in the sensing depth estimation. Because ISW extracts the large sensitivity of microwave with the lower frequency to SSM, the soil sensing depth of this method is assumed to be almost identical to that of 6.925 GHz. Considering that the difference of the soil sensing depths between two frequencies is often less than 1 cm, it can reasonably be assumed that the soil wetness between two sensing depths is homogeneous. However, the ambiguity of the sensing depth due to the use of dual-frequency brightness temperatures is a limitation of ISW. The difference of the original footprint size between different frequencies is a limitation of ISW. In addition, brightness temperatures in a higher frequency are affected by cloud water, although evidence for significant degradation of the retrieval skill due to atmospheric conditions cannot be found in the literature. Please note that ISW is also affected by surface soil roughness and VWC. PI has widely been used to monitor VWC (see [1], [3], [8], [13], [17], [18], [20], [32]) since the difference between the brightness temperatures of vertical and horizontal polarizations is reduced by the extinction process within the vegetation layer. By using the ISW and PI, the effect of the uncertainties in the surface and canopy temperatures can be minimized.

These two indices were used to retrieve SSM and VOD; same as for the JAXA standard algorithm [20]. Fig. 2 shows an overview of the PI- and ISW-based SSM and VOD retrieval algorithms. There are two loops (the SSM and VOD loops) in this algorithm. In the VOD loop, the VOD was gradually changed from 0 to 2.5 in increments of 0.025, and the RTM described above was run to obtain the brightness temperatures. The estimated PIs were then compared with those observed from the satellite sensor. The optimal VOD that minimizes the square difference (difference in Fig. 2) between the estimated and observed PIs was chosen. In the SSM loop, the SSM was gradually changed from 0.005 to 0.5 in increments of 0.005 and the RTM was run with the VOD estimated in the VOD loop. The estimated ISWs were compared with those observed from the satellite sensor. The SSM that minimized the square difference (difference in Fig. 2) between the estimated and observed ISWs was then chosen.

To obtain the optimal SSM and VOD, these two loops were iterated. First, the VOD loop was run to estimate the VOD that can reproduce the observed PI. Second, the SSM loop was run with estimated VOD to obtain the SSM that can reproduce the observed ISW. Then, the VOD loop was run again with the SSM estimated by the previous SSM loop. This process was repeated until both SSM and VOD do not change in the two loops. This retrieval method is similar to the LPRM method [1] and mostly identical to [18]. In this paper, ISW was used in the SSM loop while Sawada *et al.* [18] directly compared the estimated brightness temperatures with the observed brightness temperatures. Since our problem to be solved is relatively simple, it was easy to search the global minimum. Please note that there are many alternatives to solve the inversion problem of the RTM such as a lookup table method (see [20]).

C. Effect of Surface Soil Roughness

Following [18], an idealized experiment was implemented to quantify the impact of the surface soil roughness bias. Here, the "true" roughness parameters and the "biased" roughness parameters of the RTM are arbitrarily chosen. How the retrieval algorithm degrades due to the bias of the roughness parameters is discussed. First, the VOD value was gradually changed from 0 to 1 (but with SSM fixed) and the RTM run using the "reference" (or "true") surface soil roughness parameters to generate the model-calculated brightness temperatures. The combination of these VODs and the model-calculated brightness temperatures was then used as a surrogate of the truth in the next step. Second, the SSM and VOD retrieval algorithms described in Section III-B were run with the "smooth" surface soil roughness parameters (σ = 0.1 [cm], l = 1.5 [cm]), which is arbitrarily determined, by using the brightness temperatures generated in the first step. This "smooth" surface soil roughness parameters are biased compared with the "reference" surface soil roughness parameters. The retrieved VOD was then compared with the surrogate of the truth. Fig. 3 provides the schematic of this idealized experiment.

Red circles in Fig. 4(a) show the result of this idealized experiment when the "reference" surface soil roughness is set to the same values as the "smooth" surface soil roughness (σ = 0.1 [cm], l = 1.5 [cm]). In this case, estimated VOD is completely consistent to a surrogate of the truth. The estimated SSM is also consistent to the fixed value which is used to generate the brightness temperatures. Conversely, triangles in Fig. 4(a) show the selected result of the idealized experiment if larger σ than the "smooth" surface and fixed l (=1.5 [cm]) were chosen as a "reference" soil roughness

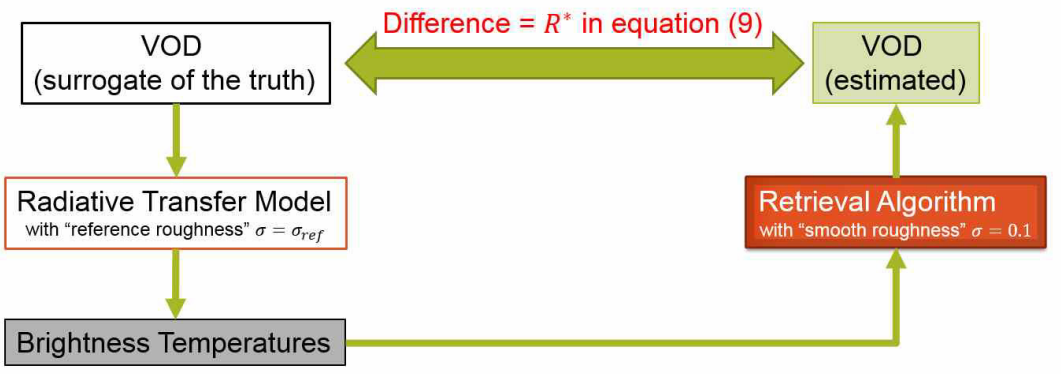

Fig. 3. Schematic of the idealized experiment. The box of "Retrieval Algorithm" is identical to what is shown in the entire Fig. 2. See Section III-C for details.

parameter. In this "rough" surface case (the true surface is rougher than expected), estimated VOD (and SSM) was not consistent to a surrogate of the truth [Fig. 4(a)], because there is a bias of σ in the retrieval algorithm.

Sawada *et al.* [18] have found that the effect of the bias in the surface soil roughness on the VOD retrieval can be defined as a constant value. So if VOD is retrieved with a smoother surface soil roughness condition than reality in the RTM, VOD can be formulated as

$$\xi = \mathrm{VOD} + R^* = b \times \mathrm{VWC} + R^* \tag{9}$$

where ξ is the biased VOD, which can be decomposed into the unbiased VOD correlated linearly with VWC [33] and the effect of surface soil roughness (R^*). This paper supports this result, although in the case that the "reference" surface soil roughness parameter σ is very large, (9) is violated with VOD < 0.3 [Fig. 4(a)]. The roughness bias degrades the skill of SSM retrievals, and the effect of SSM bias on the VOD retrieval is large in the case of a small VOD. Therefore, (9) is violated due to the bias of SSM retrieval with the extremely large roughness bias and small VOD.

In this idealized experiment, R^* was calculated as the averaged difference between estimated VOD [vertical axis in Fig. 4(a)] and the true VOD [horizontal axis in Fig. 4(a)] in the case that true VOD is larger than 0.3. Please note that the data with VOD < 0.3 can also be used to calculate R^* if the "reference" surface soil roughness is not extremely large. Fig. 4(b) shows the relationship between the "reference" surface soil roughness parameter σ and R^*. The relationship does not strongly depend on the fixed soil moisture value that was used to generate a surrogate of truth. In this paper, it was assumed that soil moisture is 0.15 [m^3/m^3] and that rms roughness height can be approximated by a linear relationship with R^*

$$\sigma_{\mathrm{reference}} = 1.1361 \times R^* + 0.1387 \tag{10}$$

where $\sigma_{\mathrm{reference}}$ is the rms height [cm] of the "reference" (correct) surface soil roughness parameter.

D. Microwave and Optical Fusion Approach

Here, the strategy to get the value of R^* and correct the rms height σ of the RTM in the real-world application is presented. Paloscia and Pampaloni [8] suggested the following relationship between VWC and LAI:

$$\mathrm{VWC} = \exp\left(\frac{\mathrm{LAI}}{y}\right) - 1 \approx \frac{\mathrm{LAI}}{y} \tag{11}$$

where y is a species-dependent parameter that represents the ratio between the leaf and stem water contents, which it is difficult to observe at satellite footprint scales. Linearization was proposed by Sawada *et al.* [18]. Substituting (11) into (9) yields

$$\xi = \frac{b}{y}\mathrm{LAI} + R^*. \tag{12}$$

The value of R^* in (12) can be estimated as the y-intercept of a linear regression of ξ and LAI.

The procedure of this Microwave and Optical Fusion Approach (MiOFA) is as follows (see also Fig. 5).

1) The retrieval algorithm described in Section III-B is run with the "smooth" surface soil roughness ($\sigma = 0.1$, $l = 1.5$) to get ξ.
2) The linear regression of ξ and LAI observed by an optical sensor is obtained to get R^*.
3) The value of σ is corrected by using R^* and (10).
4) The retrieval algorithm is run again using the corrected σ to get SSM and VOD.

To get VWC, the linear relationship between VOD and VWC proposed by Jackson and Schmmuge [33] is used. However, the uncertainty of the "b-parameter" in (9) has to be considered. Sawada *et al.* [18] found that this b-parameter did not strongly depend on the crop type at 6.925 GHz. However, the value highly depends on the assumption of a single scattering albedo of the canopy since the equifinality problem exists in the calibration of these two parameters. (A result with a large b-parameter and a large albedo is similar to that with a small b-parameter and a small albedo.) Sawada *et al.* [18] calculated the appropriate b-parameter with many values of single scattering albedo using *in situ* observation data. In this paper, the single scattering albedo was set to 0.06, which is similar to the value used in the JAXA algorithm [20]. In this case, Sawada *et al.* [18] suggested the b-parameter be approximately 0.74 at 6.9 GHz. This value is reasonable when compared with the synthesis study of [33]. Thus, a value of $b = 0.74$ was applied here, but please note that there is uncertainty of this parameter and the

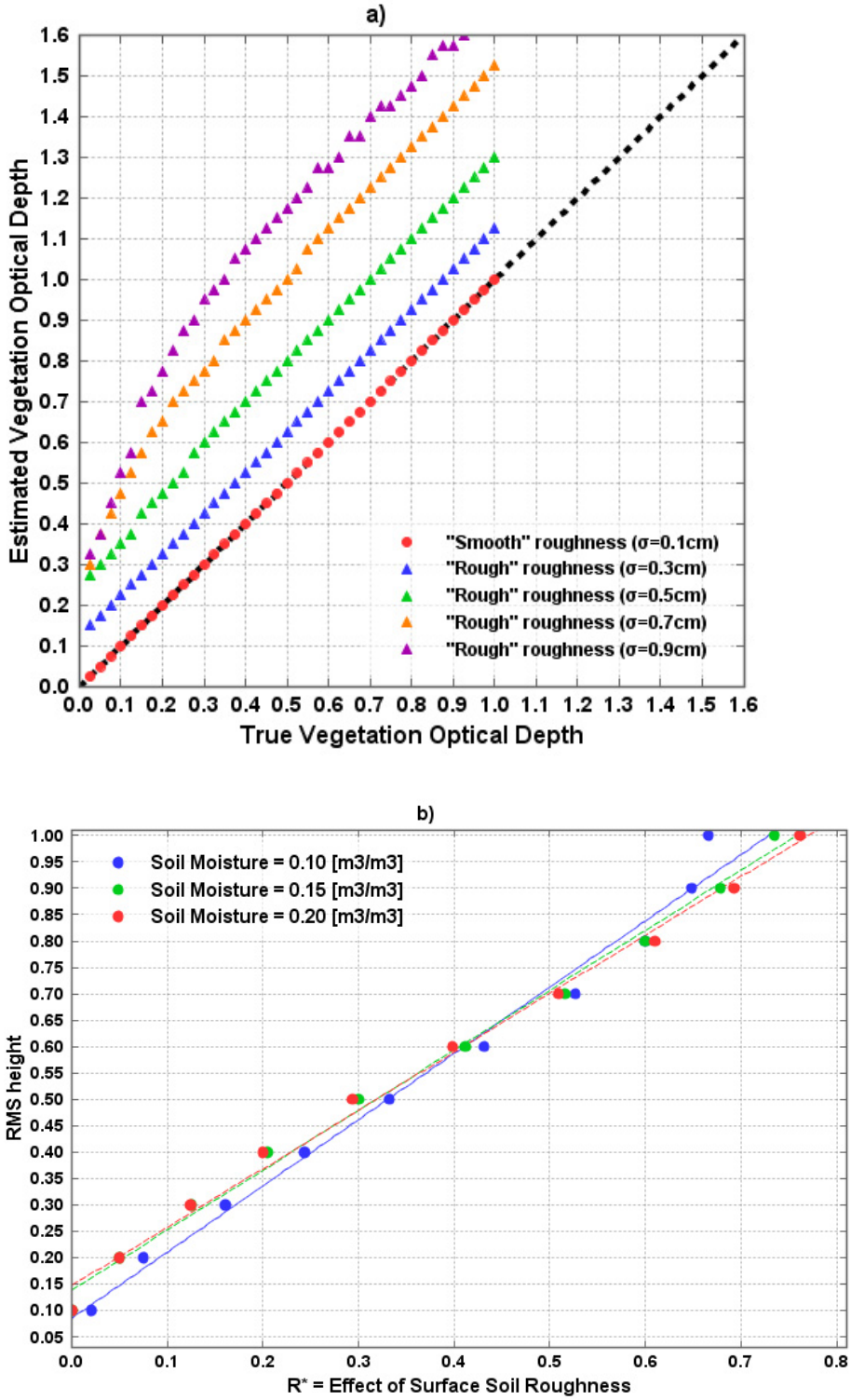

Fig. 4. (a) Sample of results from the synthetic experiment with various "reference" surface soil roughness parameters. Soil moisture is set to 0.15 [m^3/m^3] when a surrogate of the truth is generated. Red circles are the results in the case that the "reference" surface soil roughness parameters are the same as those used in the retrieval algorithm. Blue, green, yellow, and purple triangles are the results in the case that the "reference" surface soil roughness parameters are rougher than those used in the retrieval algorithm. (σ is 0.3, 0.5, 0.7, and 0.9 [cm], respectively.) (b) Relationship between "reference" soil roughness parameters and magnitude of soil surface roughness contamination to vegetation-oriented signals R^* [see (9)] in the idealized experiment. Soil moisture is set to 0.1 (blue dots), 0.15 (green dots), and 0.20 (red dots) [m^3/m^3] when a surrogate of the truth was generated. Dashed lines show the linear regressions. See Section III-C for details of the idealized experiment.

subsequent VWC estimations. LPRM VOD-based VWC was also calculated by using $b = 0.74$.

It is extremely difficult to objectively determine the value of the single scattering albedo, which brings the uncertainty to these retrievals. Although the single scattering albedo spatially and temporally changes, in this paper, the fixed value is assumed as in many operational retrieval algorithms [20], [23]. In addition, the dependence of the single scattering albedo

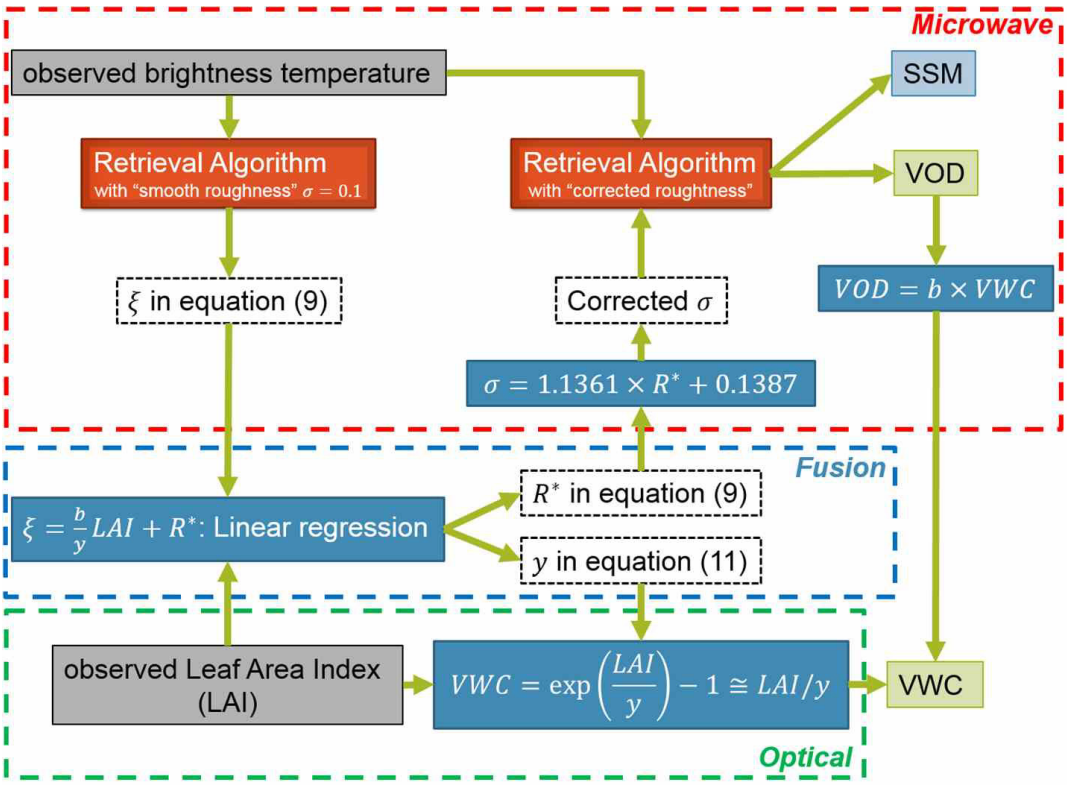

Fig. 5. Schematic of the MiOFA. See Section III-D for details.

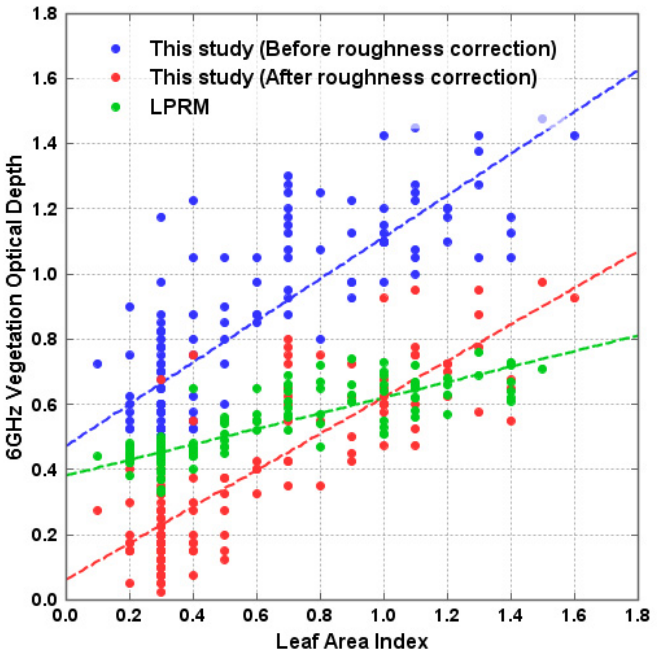

Fig. 6. Relationship between LAI and VOD in a 6.925-GHz microwave region. Blue and red circles are the result from this study with a "smooth" surface soil roughness parameter and a corrected surface soil roughness parameter given by the MiOFA method, respectively. Green circles are the result from LPRM. The dashed lines show the linear regressions.

to polarizations and frequencies is neglected although the MiOFA uses the multipolarized and multifrequency brightness temperatures. Please note that the single scattering albedo used here should be considered as an "effective albedo" [34] and that it is not simply correlated with the strength of the vegetation volume scattering because the multiple scattering is neglected in the tau–omega model. When the tau–omega model is applied to the 36.5-GHz brightness temperature, the relatively small single scattering albedo shown above can be used despite the strong vegetation volume scattering, because the effect of a multiscattering term, which is neglected by the tau–omega framework, needs to be implicitly included.

This proposed MiOFA algorithm also enables VWC to be estimated from optically observed LAI data, because the y-parameter of (11) can be obtained from the linear regression expressed by (12) when assuming that the b-parameter is fixed (see also Fig. 5). This LAI-based VWC retrieval is also evaluated in Section IV.

It should be noted that MiOFA has both similarities and differences from the JAXA standard algorithms. Both algorithms used the PI- and ISW-based retrieval strategies. While the JAXA standard algorithm considers the vegetation fractional coverage, MiOFA assumes homogeneous vegetation coverage. While the JAXA standard algorithm assumes globally fixed surface soil roughness parameters which are manually calibrated in a specific site, MiOFA determines them objectively.

IV. Results

Point scale application and evaluation of MiOFA at the Yanco region (Fig. 1) during 2013–2014 are presented. How MiOFA works in a real-world application is first presented using a scatterplot of estimated VOD and MODIS LAI. The time series of VWC and SSM from MiOFA, JAXA standard algorithm (hereafter simply called JAXA), LPRM, and the *in situ* observations are then presented, and the performance

of MiOFA to simultaneously retrieve SSM and VWC is discussed.

Blue circles in Fig. 6 indicate the relationship between MODIS LAI and VOD (or ξ) retrieved with a "smooth" surface soil roughness parameter. There is a contradiction between MODIS LAI and VOD because VOD has a high value with LAI = 0. This is due to the bias of the roughness parameter of the RTM as discussed in Section III-C. Green circles in Fig. 6 show that LPRM VOD and MODIS LAI also have this contradiction probably due to the assumption of a smooth surface soil roughness of the RTM [1].

According to the linear regression of the VOD and LAI (dashed blue line in Fig. 6), it was found that R^* is 0.473. From (10), the corrected rms height σ of this site is 0.677 [cm]. By using this rms height, the retrieval algorithm was run again to get the unbiased VOD displayed as red circles in Fig. 6. The contradiction between MODIS LAI and VOD no longer exists. Results of the biased VODs (ξ) (>0.6 in most cases), the unbiased VOD (>0.2 in most cases), and the corrected rms height (<0.7 cm) indicate that in this case, the MiOFA works in the range in which (9) was valid [see Fig. 4(a)].

Fig. 7(a) shows the time series of the estimated and observed VWCs. The roughness correction by MiOFA has a tremendous impact on the retrieved VWC. The VWC retrieved from this study with a "smooth" surface soil roughness parameter and LPRM have high values (>0.50 [kg/m^2]) in the dry season when LAI is less than 0.3, due to the contradiction in Fig. 6. Moreover, this high VWC is not consistent with *in situ* observations. The roughness correction by the MiOFA significantly decreases the retrieved VWC by eliminating the roughness contamination to vegetation-oriented signals. Compared to *in situ* observations, MiOFA improved the VWC retrieval skill. However, the MiOFA may have overestimated VWC. Possible reasons of this overestimation are the heterogeneity of VWC in the satellite footprint scale [see whiskers and differences between observations of different types in Fig. 7(a)], the uncertainty of the b-parameter and single scattering albedo as discussed in Section III-D, and the simplification of the canopy radiative transfer using the zero-order model. It should be noted that since the number of *in situ* VWC observations is small, no statistical metrics were calculated.

Fig. 7(b) and (c) shows that the roughness correction by the MiOFA strongly affects the SSM retrieval. Please note that there are two pathways to change the estimated SSM by the MiOFA: changing the emissivity of the soil by increasing the rms height, and changing the emissivity of the canopy by decreasing the VOD. As a result, when the rms height is increased by the MiOFA, the range of the fluctuations of SSM is decreased [compare black triangles with blue circles in Fig. 7(b) and (c)]. Compared to the *in situ* observed SSM, the MiOFA improved the performance of retrieving SSM in rms error (RMSE) and correlation coefficient (R) (Table I). However, the MiOFA increased the bias of SSM by roughness correction (Table I). Before roughness correction, the algorithm overestimates SSM in wet periods and underestimates SSM in dry periods. Because this overestimation and underestimation offset each other, the bias of the algorithm before roughness correction was relatively small. Therefore, the MiOFA cannot improve the bias score while decreasing RMSE. The performances indicated in Table I are similar to those shown in the other validation studies [see 14]. Table I indicates that the new algorithm of this paper outperformed descending (nighttime) LPRM and JAXA products in three metrics.

TABLE I

PERFORMANCE OF SSM RETRIEVAL ALGORITHMS USING THE DESCENDING (NIGHTTIME) 6.925- AND 36.5-GHZ DATA[a]

	this study (after roughness correction)	this study (before roughness correction)	LPRM	JAXA
RMSE [m^3/m^3]	0.070	0.088	0.199	0.073
BIAS[m^3/m^3]	0.038	0.013	-0.178	0.053
R	0.441	0.438	0.372	0.299

[a]RMSE is a root mean squared error. R is a correlation coefficient.

Fig. 8 shows the VWC time series calculated from LAI using (11), with an estimated y-parameter of 1.16. From the linear regression of (11), the slope b/y can be obtained. Because the value of b-parameter (0.74) is given, the value of y can be obtained. Performance of the LAI-based VWC retrieval is similar to that of the VOD-based VWC retrieval. Moreover, the relationship between optically observed vegetation indices (e.g., LAI and NDVI) and VWC highly depends on the vegetation type (see [35], [36]), which makes it difficult to observe VWC using optical sensors. Thus, the fact that MiOFA can explicitly estimate the parameter of the LAI–VWC relationship without any *in situ* training data is significant.

V. DISCUSSION AND CONCLUSION

The uncertainty of surface soil roughness greatly deteriorates the performance of SSM and VWC retrieval from passive microwave observations. By fusing microwave observations from AMSR2 and optical vegetation observations from MODIS, the bias of surface soil roughness can be removed and the VWC retrieval skill can greatly be improved. The VWC can quantitatively be estimated by eliminating the contamination of the time-invariant surface soil roughness effects to VOD. Although the fundamental idea has been proposed in [18], it relied on the *in situ* observed brightness temperatures and LAI. In this paper, it is verified that this approach can also be applied to satellite data. This is the first satellite SSM and VWC retrieval algorithms that can objectively determine the value of the surface soil roughness parameter in the RTM.

Since both VOD and LAI easily saturate in the moderate and dense vegetation areas, the semiarid region with the sparse vegetation cover is the most appropriate regions where the MiOFA is applied. The MiOFA can be applied to the regions characterized by high cloud coverages. Once the linear regression between VOD and LAI is obtained, LAI optical observations are not needed for the retrieval. Therefore, the linear regression using cloud-free VOD and LAI observations is first provided and then temporally fine VWC data can

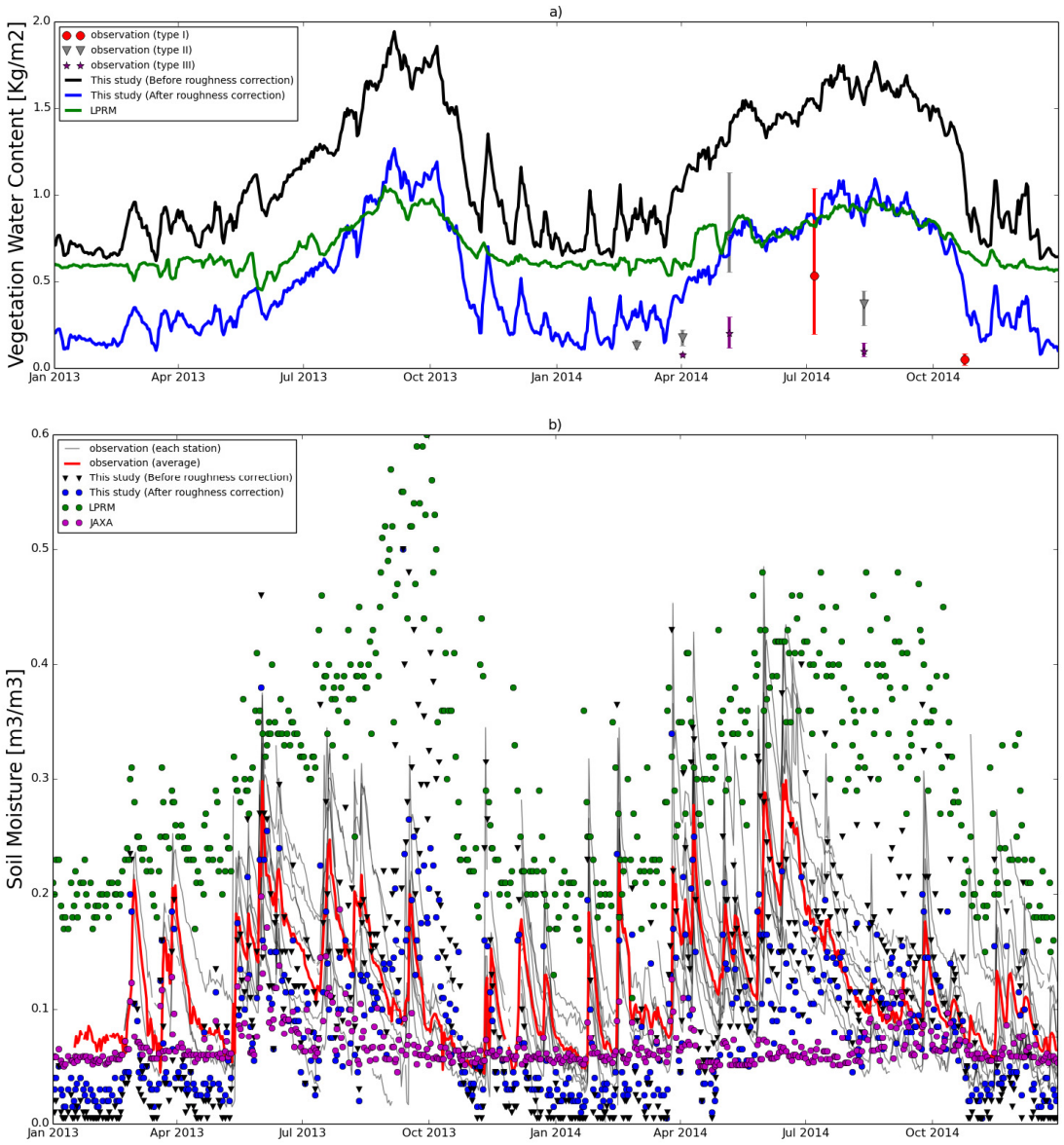

Fig. 7. (a) Time series of VWC. Black and blue lines are a five-day running mean of VWC from this study with a "smooth" surface soil roughness parameter and a corrected surface soil roughness parameter by the MiOFA method, respectively. The green line is a five-day running mean of VWC from the LPRM. Red circles, gray triangles, and purple stars are the *in situ* observed VWC, calculated as an average of VWC measurements at all observation plots of Type I, Type II, and Type III field surveys, respectively (see Section II). Whiskers show the maximum and minimum VWCs among the observation plots. (b) Time series of SSM. Black triangles and blue circles are SSM from this study with a "smooth" surface soil roughness parameter and a corrected surface soil roughness parameter by the MiOFA method (using 6.925 and 36.5 GHz), respectively. Purple and green circles are SSM from the JAXA standard algorithm and LPRM (using 6.925 GHz), respectively. Gray lines are SSM from *in situ* observation sites of the Yanco observation network, and the red line is the mean of them.

be generated using microwave signals. This strategy can overcome the limitation of temporally sparse optical LAI observations due to clouds. For global applications, globally fixed vegetation parameters (e.g., *b*-parameter) can be problematic, although this assumption has widely been used in the existing global retrieval algorithms. Sawada *et al.* [18] obtained the ground truth which supports this assumption to some extent. Evaluating the global applicability of our new MiOFA method will be a focus of our future work.

Although some positive impacts of the MiOFA on the SSM estimation are detected, the improvement of SSM retrieval skill by roughness correction is not significant. To further improve the SSM retrieval skill, understanding of the uncertainties of sensing depths, single scattering albedo, and spatial heterogeneity in the large footprint should be improved.

One of the by-products of MiOFA is the surface soil roughness parameter. Wang *et al.* [19] has already estimated their surface soil roughness parameter globally and identified that their estimated values are correlated with vegetation types and topography. By analyzing the global distribution of the surface soil roughness parameter derived here, the understanding of the source of surface soil roughness in the passive microwave radiative transfer can be improved. It should be noted that the spatial representativeness of surface soil roughness is uncertain, and it is extremely difficult to obtain satellite footprint-scale surface roughness *in situ* observations.

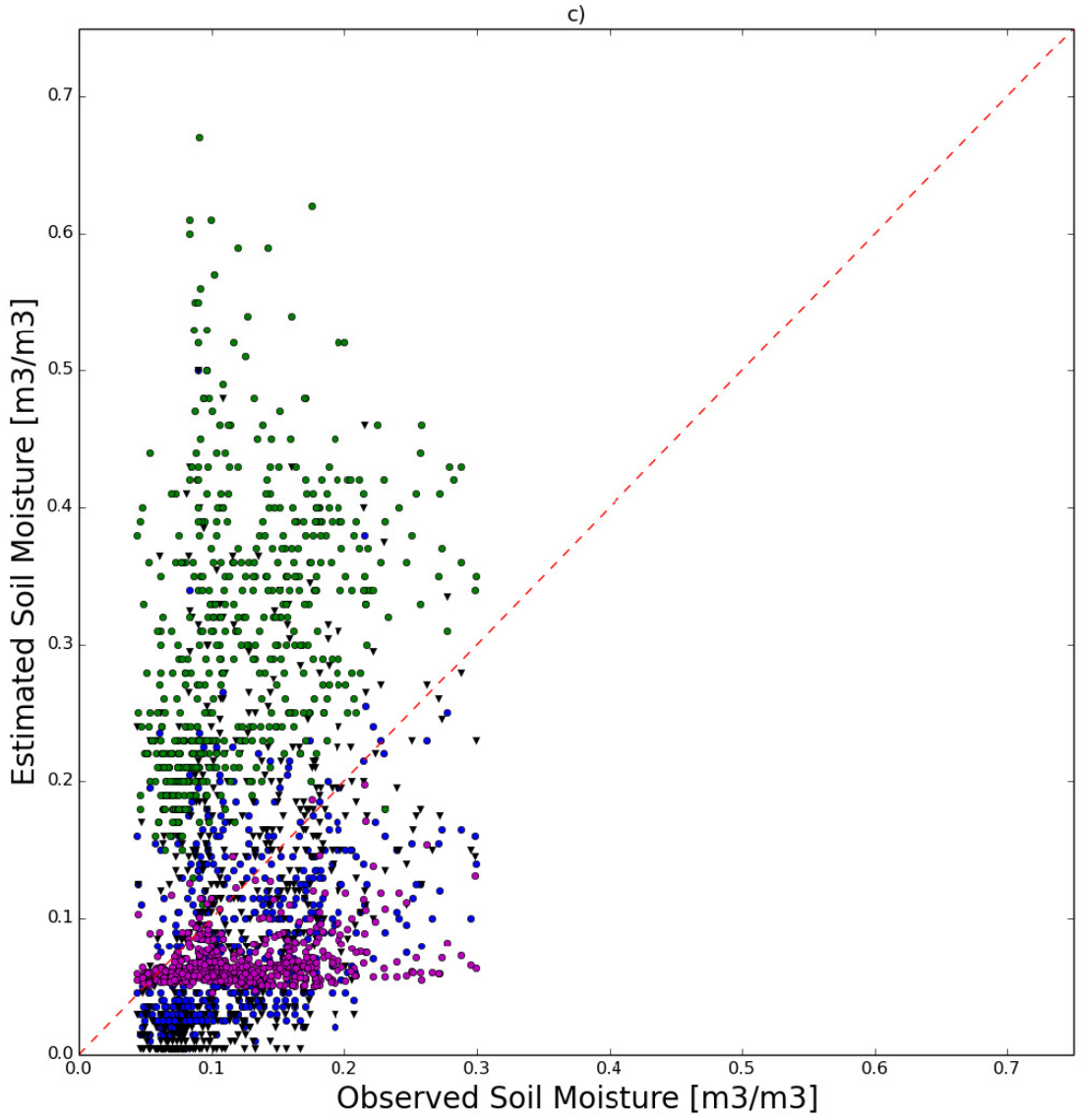

Fig. 7. *(Continued)* (c) Scatter plot of SSM retrieval. Black triangles and blue circles are SSM from this study with a "smooth" surface soil roughness parameter and a corrected surface soil roughness parameter by the MiOFA method (using 6.925 and 36.5 GHz), respectively. Purple and green circles are SSM from the JAXA standard algorithm and LPRM (using 6.925 GHz), respectively.

In addition, the exact physical relationship between these parameters and real-world soil roughness is unclear. Therefore, it is currently impossible to validate the tuned surface soil roughness parameters by *in situ* observations.

The other by-product of MiOFA is the y-parameter of the relationship between LAI and VWC [see (11)]. This parameter indicates the structure of vegetation and is a proxy of the ratio of leaf wet biomass to total aboveground wet biomass. Therefore, by analyzing the global distribution of the estimated y-parameter and its changes, understanding of the global ecosystem structure and its changes can be improved.

Although AMSR2 brightness temperatures were used in this paper, the theory and strategy described here can be transferred to other microwave satellite missions such as the SMOS and Soil Moisture Active Passive missions. Therefore, the findings of this paper may contribute to the wider community of earth surface observations using microwave signals.

ACKNOWLEDGMENT

Surface soil moisture ground observation was furnished by Monash University. All ground observation data can be made available upon request to the authors, and soil moisture network data can be downloaded at http://www.oznet.org.au/. The AMSR2 brightness temperature and surface soil moisture products were provided by JAXA and can be downloaded at https://gcom-w1.jaxa.jp/auth.html. The LPRM surface soil moisture and VOD product, and the MODIS-derived LAI product were provided by NASA and can be downloaded at https://earthdata.nasa.gov/. The authors would like to thank F. Winston, A. Monerris, M. S. Yee, and X. Wu for their field work contributions, N. Ye for his assistance with field

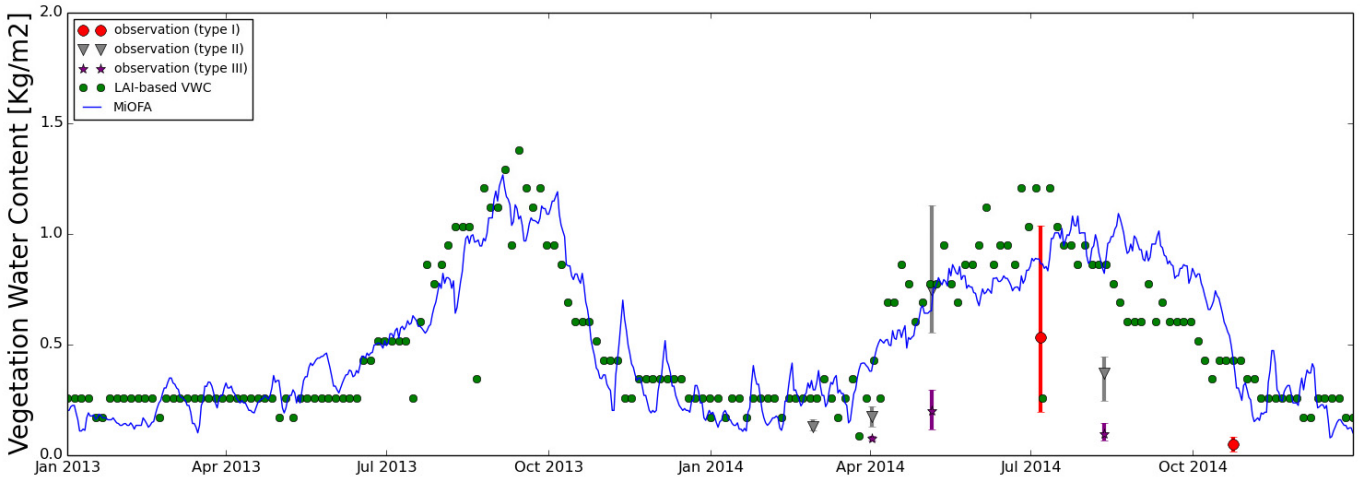

Fig. 8. Time series of VWC retrieved from optically sensed LAI (green dots) and MiOFA (blue lines; same as Fig. 7). Red circles, gray triangles, and purple stars are the *in situ* observed VWC which is calculated as an average of VWCs at all observation plots of Type I, Type II, and Type III field surveys, respectively (see Section II). Whiskers show the maximum and minimum VWCs among the observation plots.

measurements and comments to this manuscript, C. Rudiger for sharing his *in situ* vegetation water content data, and the associate editor and anonymous reviewers for their helpful comments.

REFERENCES

[1] M. Owe, R. D. Jeu, and J. Walker, "A methodology for surface soil moisture and vegetation optical depth retrieval using the microwave polarization difference index," *IEEE Trans. Geosci. Remote Sens.*, vol. 39, no. 8, pp. 1643–1654, Aug. 2001.

[2] A. Shibata, K. Imaoka, and T. Koike, "AMSR/AMSR-E level 2 and 3 algorithm developments and data validation plans of NASDA," *IEEE Trans. Geosci. Remote Sens.*, vol. 41, no. 2, pp. 195–203, Feb. 2003.

[3] E. G. Njoku, T. J. Jackson, V. Lakshmi, T. K. Chan, and S. V. Nghiem, "Soil moisture retrieval from AMSR-E," *IEEE Trans. Geosci. Remote Sens.*, vol. 41, no. 2, pp. 215–229, Feb. 2003.

[4] X. Yuan, Z. Ma, M. Pan, and C. Shi, "Microwave remote sensing of short-term droughts during crop growing seasons," *Geophys. Res. Lett.* vol. 42, no. 11, pp. 4394–4401, 2015, doi: 10.1002/2015GL064125.

[5] C. M. Taylor, R. A. M. de Jeu, F. Guichard, P. P. Harris, and W. A. Dorigo, "Afternoon rain more likely over drier soils," *Nature*, vol. 489, pp. 423–426, Sep. 2012, doi: 10.1038/nature11377.

[6] J. P. Walker and P. R. Houser, "A methodology for initializing soil moisture in a global climate model: Assimilation of near-surface soil moisture observations," *J. Geophys. Res. Atmos.*, vol. 106, pp. 11761–11774, Jun. 2001, doi: 10.1029/2001JD900149.

[7] Z. Su, P. de Rosnay, J. Wen, L. Wang, and Y. Zeng, "Evaluation of ECMWF's soil moisture analyses using observations on the Tibetan Plateau," *J. Geophys. Res. Atmos.*, vol. 118, no. 11, pp. 5304–5318, 2013, doi: 10.1002/jgrd.50468.

[8] S. Paloscia and P. Pampaloni, "Microwave polarization index for monitoring vegetation growth," *IEEE Trans. Geosci. Remote Sens.*, vol. 26, no. 5, pp. 617–621, Sep. 1988.

[9] Y. Y. Liu *et al.*, "Recent reversal in loss of global terrestrial biomass," *Nature Climate Change*, vol. 5, pp. 470–474, Mar. 2015, doi: 10.1038/nclimate2581.

[10] L. Zhou *et al.*, "Widespread decline of Congo rainforest greenness in the past decade," *Nature*, vol. 509, pp. 86–90, Apr. 2014, doi: 10.1038/nature13265.

[11] Y. Sawada and T. Koike, "Simultaneous estimation of both hydrological and ecological parameters in an ecohydrological model by assimilating microwave signal," *J. Geophys. Res. Atmos*, vol. 119, no. 14, pp. 8839–8857, 2014, doi: 10.1002/2014JD021536.

[12] Y. Sawada, T. Koike, and J. P. Walker, "A land data assimilation system for simultaneous simulation of soil moisture and vegetation dynamics," *J. Geophys. Res. Atmos.*, vol. 120, no. 12, pp. 5910–5930, 2015, doi: 10.1002/2014JD022895.

[13] E. Santi, S. Pettinato, S. Paloscia, P. Pampaloni, G. Macelloni, and M. Brogioni, "An algorithm for generating soil moisture and snow depth maps from microwave spaceborne radiometers: HydroAlgo," *Hydrol. Earth Syst. Sci.*, vol. 16, pp. 3659–3676, Oct. 2012, doi: 10.5194/hess-16-3659-2012.

[14] T. J. Jackson *et al.*, "Validation of advanced microwave scanning radiometer soil moisture products," *IEEE Trans. Geosci. Remote Sens.*, vol. 48, no. 12, pp. 4256–4272, Dec. 2010, doi: 10.1109/TGRS.2010.2051035.

[15] M. Neelam and B. P. Mohanty, "Global sensitivity analysis of the radiative transfer model," *Water Resour. Res.*, vol. 51, no. 4, pp. 2428–2443, Apr. 2015, doi: 10.1002/2014WR016534.

[16] J. Patton and B. Hornbuckle, "Initial validation of SMOS vegetation optical thickness in iowa," *IEEE Geosci. Remote Sens. Lett.*, vol. 10, no. 4, pp. 647–651, Jul. 2013, doi: 10.1109/LGRS.2012.2216498.

[17] E. G. Njoku and S. K. Chan, "Vegetation and surface roughness effects on AMSR-E land observations," *Remote Sens. Environ.*, vol. 100, no. 2, pp. 190–199, 2006, doi: 10.1016/j.rse.2005.10.017.

[18] Y. Sawada, H. Tsutsui, T. Koike, M. Rasmy, R. Seto, and H. Fujii, "A field verification of an algorithm for retrieving vegetation water content from passive microwave observations," *IEEE Trans. Geosci. Remote Sens.*, vol. 54, no. 4, pp. 2082–2095, Apr. 2016, doi: 10.1109/TGRS.2015.2495365.

[19] S. Wang *et al.*, "Global-scale evaluation of roughness effects on C-band AMSR-E observations," *Remote Sens.*, vol. 7, no. 5, pp. 5734–5757, 2015, doi: 10.3390/rs70505734.

[20] H. Fujii, T. Koike, and K. Imaoka, "Improvement of the AMSR-E algorithm for soil moisture estimation by introducing a fractional vegetation coverage dataset derived from MODIS data," *J. Remote Sens. Soc. Japan*, vol. 29, no. 1, pp. 282–292, 2009.

[21] M. Kachi, K. Naoki, M. Hori, and K. Imaoka, "AMSR2 validation results," in *Proc. IEEE Int. Geosci. Remote Sens. Symp. (IGARSS)*, Jul. 2013, pp. 831–834, doi: 10.1109/IGARSS.2013.6721287.

[22] Y. Y. Liu, R. A. M. de Jeu, M. F. McCabe, J. P. Evans, and A. I. J. M. van Dijk, "Global long-term passive microwave satellite-based retrievals of vegetation optical depth," *Geophys. Res. Lett.*, vol. 38, no. 18, p. L18402, 2011, doi: 10.1029/2011GL048684.

[23] M. Owe, R. de Jeu, and T. Holmes, "Multisensor historical climatology of satellite-derived global land surface moisture," *J. Geophys. Res.*, vol. 113, p. F01002, Mar. 2008, doi: 10.1029/2007JF000769.

[24] D. Huang *et al.*, "Stochastic transport theory for investigating the three-dimensional canopy structure from space measurements," *Remote Sens. Environ.*, vol. 112, no. 1, pp. 35–50, 2008.

[25] A. B. Smith *et al.*, "The Murrumbidgee soil moisture monitoring network data set," *Water Resour. Res.*, vol. 48, no. 7, p. W07701, 2012.

[26] M. S. Yee, J. P. Walker, A. Monerris, C. Rüdiger, and T. J. Jackson, "On the identification of representative *in situ* soil moisture monitoring stations for the validation of SMAP soil moisture products in Australia," *J. Hydrol.*, vol. 537, pp. 367–381, Jun. 2016.

[27] D. N. Kuria, T. Koike, H. Lu, H. Tsutsui, and T. Graf, "Field-supported verification and improvement of a passive microwave surface emission model for rough, bare, and wet soil surfaces by incorporating shadowing effects," *IEEE Trans. Geosci. Remote Sens.*, vol. 45, no. 5, pp. 1207–1216, May 2007, doi: 10.1109/TGRS.2007.894552.
[28] M. C. Dobson, F. T. Ulaby, M. T. Hallikainen, and M. A. El-Rayes, "Microwave dielectric behavior of wet soil—Part II: Dielectric mixing models," *IEEE Trans. Geosci. Remote Sens.*, vol. GE-23, no. 1, pp. 35–46, Jan. 1985.
[29] F. Ulaby, R. K. Moore, and A. Fung, *Microwave Remote Sensing: Active and Passive—Volume Scattering and Emission Theory*, vol. 3. Norwood, MA, USA: Artech House, 1986.
[30] T. Mo, B. J. Choudhury, T. J. Schmugge, J. R. Wang, and T. J. Jackson, "A model for microwave emission from vegetation-covered fields," *J. Geophys. Res.*, vol. 87, pp. 11229–11237, Dec. 1982.
[31] A. A. Chukhlantsev, *Microwave Radiometry of Vegetation Canopies*. Dordrecht, The Netherlands: Springer, 2006.
[32] T. Koike *et al.*, "Development of an advanced microwave scanning radiometer (AMSR-E) algorithm of soil moisture and vegetation water content," (in Japanese), *Annu. J. Hydraulic Eng.*, vol. 48, p. 217, Jan. 2004.
[33] T. J. Jackson and T. J. Schmmuge, "Vegetation effects on the microwave emission of soils," *Remote Sens. Environ.*, vol. 36, no. 3, pp. 203–212, 1991.
[34] M. Kurum, "Quantifying scattering albedo in microwave emission of vegetated terrain," *Remote Sens. Environ.*, vol. 129, pp. 66–74, Feb. 2013, doi: 10.1016/j.rse.2012.10.021.
[35] Y. Gao, J. P. Walker, M. Allahmoradi, A. Monerris, D. Ryu, and T. J. Jackson, "Optical sensing of vegetation water content: A synthesis study," *IEEE J. Sel. Topics Appl. Earth Observat. Remote Sens.*, vol. 8, no. 4, pp. 1456–1464, Apr. 2015.
[36] M. T. Yilmaz, E. R. Hunt, Jr., and T. J. Jackson, "Remote sensing of vegetation water content from equivalent water thickness using satellite imagery," *Remote Sens. Environ.*, vol. 112, no. 5, pp. 2514–2522, 2008, doi: 10.1016/j.rse.2007.11.014.

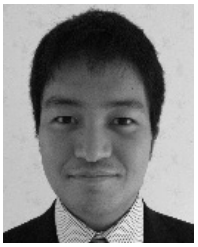

Yohei Sawada received the B.Eng., M.Eng., and Ph.D. degrees from The University of Tokyo, Tokyo, Japan, in 2011, 2013, and 2016, respectively.

He was a Post-Doctoral Researcher at the RIKEN Advanced Institute for Computational Science, Kobe, Japan. He is currently a Researcher with the Meteorological Research Institute, Japan Meteorological Agency, Tsukuba, Japan. His research interests include the data assimilation, microwave remote sensing, and drought monitoring and prediction.

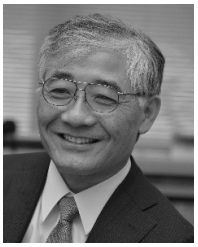

Toshio Koike received the bachelor's, master's, and Doctor of Engineering degrees from The University of Tokyo, Tokyo, Japan, in 1980, 1982, and 1985, respectively.

He became a Research Associate at The University of Tokyo, in 1985, and was a Lecturer from 1986 to 1987. He was an Associate Professor at the Nagaoka University of Technology, Nagaoka, Japan, from 1988 to 1999, and became a Professor in 1999. In 1999, he joined the Department of Civil Engineering, The University of Tokyo, where he held the position of Professor until 2017. He is currently an Emeritus Professor with The University of Tokyo, and an Executive Director of the International Centre for Water Hazard and Risk Management under the auspices of UNESCO, Tsukuba, Japan. His research interests include the water cycle and climate sciences and their applications to water resources management, which can be classified into the following three components: the establishment of satellite remote sensing, the development of the data integration and information fusion system, and the development of the hydrological downscaling methods including satellite-based data assimilation. Aside from his scientific contributions to water cycle and climate sciences and water resources management, he has been leading the international water cycle science projects and the intergovernmental science and technology cooperation.

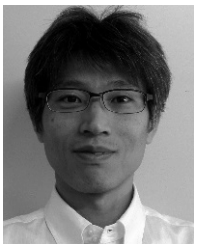

Kentaro Aida received the B.E. and M.E. degrees from the Nagaoka University of Technology, Nagaoka, Japan, in 1998 and 2000, respectively, and the Ph.D. degree from The University of Tokyo, Tokyo, Japan, in 2017.

He is currently a Project Researcher with the University of Tsukuba, Tsukuba, Japan. His research interests include the soil moisture algorithm development using the synthetic aperture radar.

Kinya Toride received the B.Eng. and M.Eng. degrees from The University of Tokyo, Tokyo, Japan, in 2014 and 2015, respectively. He is currently pursuing the Ph.D. degree in civil and environmental engineering with the University of California, Davis, CA, USA.

His research interests include the upscaled land surface modeling and the atmospheric river simulation.

Jeffrey P. Walker received the B.E. (civil) and B.Surveying (with Hons 1 and University Medal) degrees in 1995 and the Ph.D. degree in 1999 in water resources engineering, all from the University of Newcastle, Callaghan, NSW, Australia. His Ph.D. thesis focused on the early pioneering research on the estimation of root-zone soil moisture from assimilation of remotely sensed surface soil moisture observations.

He joined the NASA Goddard Space Flight Center, Greenbelt, MD, USA, to implement his soil moisture work globally. In 2001, he joined the Department of Civil and Environmental Engineering, The University of Melbourne, Melbourne, VIC, Australia, as a Lecturer, where he continued his soil moisture work, including the development of the only Australian airborne capability for simulating new satellite missions for soil moisture. In 2010, he was appointed as a Professor with the Department of Civil Engineering, Monash University, Clayton, VIC, Australia, where he is continuing this research. He is contributing to soil moisture satellite missions at NASA, ESA, and JAXA, as a Science Team Member for the Soil Moisture Active Passive mission and a Cal/Val Team Member for the Soil Moisture and Ocean Salinity and Global Change Observation Mission-Water, respectively.